

Abstract

The buckling problem represents a way to evaluate the effect of in-plane forces in the behaviour of plates. The effect is distributed along the plate domain, and thus the Boundary Element Method (BEM) formulation of the problem requires domain integration. Several techniques can be used in the numerical implementation of the BEM to replace the domain integral with equivalent boundary integrals. This study adopted the Dual Reciprocity Method (DRM) to obtain a formulation without domain integrals. The bending model considered the effect of the shear deformation for better assessment of the relationship between the buckling load and the plate thickness. The analyses considered in-plane forces distributed in one or in both directions of the plate (normal forces), as well as in the tangential direction to the plate side (shear forces). The numerical results obtained for square and rectangular plates are compared with those available in the literature.

Keywords: dual reciprocity method, plate buckling, shear deformation, Reissner plates, boundary elements.

Introduction

In-plane forces appear in the study of plates when the plate bending equilibrium includes the effect of geometrical non-linearity (GNL). In-plane forces affect the plate curvature in bending, and the reduction in the plate thickness considerably strengthens the effect of the in-plane forces on the plate behaviour. Timoshenko [1] presented a study of the equilibrium of plates under in-plane forces considering the effect of the geometrical non-linearity using the classical plate bending model. Several studies in the literature extended this development to bending models including the effect of shear deformation to analyse thin or moderately thick plates [2], and thick plates under some types of support along the plate boundary as discussed in [3]. The effect of shear deformation improves the accuracy of the plate bending model as shown by Reissner in the study of stress concentration around holes [4], or by Mindlin in wave propagation analyses [5] and carries a better assessment of the relationship between the buckling load and the plate thickness.

Nardini and Brebbia [6] studied vibration analysis using plane elements, and the domain integral was transformed into an equivalent boundary integral using the divergence theorem and an auxiliary approximating function. They did not place auxiliary points on the domain but only on the boundary. The target of that paper was not to eliminate the domain integral, but it encouraged other researchers to develop further studies where an eigenvalue problem was used to replace the domain integration [7]. The first time the name DRM was used related to the conversion of the domain integral into equivalent boundary integrals was in studies on dynamic and heat transfer problems presented in [8]. Brebbia and Nardini presented further applications of the DRM and new researchers were attracted to study this technique and extend it to several engineering applications. Partridge, Brebbia and Wrobel gave a more detailed explanation of the DRM in a book [9], which included some computer codes used in the method.

Nowadays, the DRM is widely used in several formulations to solve engineering problems, including those related to plate bending after the first study presented by Kamiya and Sawaki [10] as summarised next. Silva and Venturini [11] studied the bending of plates on elastic foundations. Sawaki, Takeuche and Kamiya [12] studied the effect of finite displacements in the bending of thin plates. Elzein and Syngellakis [13] obtained the buckling parameters for thin plates. Davies and Moslehy [14] obtained the natural frequencies and vibration modes according to the classical bending model. Lin, Duffield and Shih [15] performed studies on the buckling of rectangular and circular plates. Wen, Aliabadi and Young [16] obtained results using the direct integration method and DRM for plate bending including the effect of shear deformation and presented the linear radial basis function used in the DRM for the analysis of plates and shells including the effect of the shear deformation in [17]. Wang, Ji and Tanaka [18] presented the solution for the plate-bending problem considering the effect of finite displacements using the von Kármán equations, similarly to Wen, Aliabadi and Young [19] who have also included the effect of shear deformation in the bending model. Purbolaksono and Aliabadi [20] presented a comparison of the results obtained with the DRM versus domain integrations to account for the effect of GNL in buckling analyses using the Reissner model. Supriyono and Aliabadi [21] solved plate bending problems with the effect of the shear deformation and included effects of geometrical and physical non-linearities. Purbolaksono and Aliabadi [22] analysed large deflections in plate bending considering the effect of shear deformation. Yan, Feng and Zhou [23] presented the coupling between DRM, BEM and a meshless method for the plate solution according to the classical model. Purbolaksono, Dirgantara and Aliabadi [24] analysed crack problems in plate bending with effects of the shear deformation and geometrical non-linearities. Useche and Albuquerque [25] performed the dynamic analyses of plates with the bending model including the effect of the shear deformation. Di Pisa and Aliabadi [26] performed a study of crack growth in assembled plate structures under fatigue effects. Useche [27] performed the vibration analysis of shallow shells including the effect of the shear deformation. Pomeranz and Hamill [28] showed a comparison between the Bessel function fundamental solution and the DRM to analyse the bending of plates in an elastic foundation. Uğurlu [29] performed the vibration analysis of plates with a coupled fluid according to the classical plate theory. Useche and Albuquerque [30] carried out a dynamic analysis under the transient condition for shallow shells including the effect of the shear deformation in the bending model, while Useche and Harnish [31] presented a modal analysis for thick and shallow shells.

An alternative BEM formulation for buckling analyses in [32] employed two integrals containing the effect of GNL, with one computed in the domain and the other computed on the boundary. The use of first derivatives of the deflection in kernels of integrals related to the effect of GNL, instead of the second derivatives, and the fact that there was no need of relating the derivatives of in-plane forces were the main features of the alternative formulation. This present study concerns the application of the DRM to replace the domain integral by equivalent boundary integrals in the formulation presented in [32]. The numerical implementation employed quadratic shape functions to approximate displacements, plate rotations, distributed shears and moments in the boundary elements as implemented in [32], as well as the inverse iteration and Rayleigh quotient to compute the lowest eigenvalue with the corresponding eigenvector. Two types of radial basis functions for the DRM are considered in this study. The changes in the value of the buckling parameter according to the plate thickness of non-perforated plates are studied, and the results obtained for square and rectangular plates are compared to those in the literature.

2 Boundary Integral Equations

The present study considers a plate made of an isotropic and homogeneous material, under in-plane forces distributed in the domain, to perform buckling analyses. The well-known displacement boundary integral equations (DBIEs) for the buckling problem [33] are given next:

$$\frac{1}{2}C_{ij}(x')u_j(x') + \int_{\Gamma} [T_{ij}(x', x)u_j(x) - U_{ij}(x', x)t_j(x)]d\Gamma(x)$$

$$= \iint_{\Omega} U_{i3}(x', X) \left[\frac{\partial}{\partial X_{\alpha}} \left(N_{\alpha\beta} \frac{\partial u_3}{\partial X_{\beta}} \right) \right] d\Omega(X) \quad (1)$$

where C_{ij} is an element of the matrix C related to the boundary geometry at the source point, which becomes the identity matrix when a smooth boundary is considered, u_{α} is the plate rotation in direction α , and u_3 is the plate deflection. U_{ij} represents the rotation ($j=1, 2$) or the deflection ($j=3$) due to a unit couple ($i=1, 2$) or a unit point force ($i=3$). T_{ij} represents the moment ($j=1, 2$) or the shear ($j=3$) due to a unit couple ($i=1, 2$) or a unit point force ($i=3$). U_{ij} and T_{ij} are related to the fundamental solution. In this study, Latin indices take on values $\{1, 2 \text{ and } 3\}$ and Greek indices take on values $\{1, 2\}$.

The general constitutive equations are written next and using a unified notation for the Reissner and Mindlin plate models:

$$M_{\alpha\beta} = D \frac{(1-\nu)}{2} \left(u_{\alpha,\beta} + u_{\beta,\alpha} + \frac{2\nu}{1-\nu} u_{\gamma,\gamma} \delta_{\alpha\beta} \right) + \delta_{\alpha\beta} qRE \quad (2)$$

$$Q_{\alpha} = D \frac{(1-\nu)}{2} \lambda^2 (u_{\alpha} + u_{3,\alpha}) \quad (3)$$

with

$$\lambda^2 = 12 \frac{\kappa^2}{h^2}; \quad RE = \frac{\nu}{\lambda^2(1-\nu)}$$

The plate has a uniform thickness h , D is the flexural rigidity, ν is Poisson's ratio, q is the distributed load on the plate domain and $\delta_{\alpha\beta}$ is the Kronecker delta. The shear parameter κ^2 is equal to $5/6$ and $\pi^2/12$ for the Reissner and Mindlin models, respectively. The product qRE in eqn. (2) corresponds to the linearly weighted average effect of the normal stress component in the thickness direction, which should be considered in the Reissner model [4] but not in the Mindlin model [5]. This term is null in the buckling problem because the distributed load q is equal to zero in the analysis.

The kernel of the domain integral in eqn. (1) contains the generalised form of the effect of GNL. This kernel is usually simplified in the literature with the equilibrium equations for in-plane forces and assuming the absence of volume forces (i.e., $N_{\alpha\beta,\alpha}=0$). The second derivatives of the deflection result from the simplification, as shown in eqn. (4):

$$\iint_{\Omega} U_{i3}(x', X) \left[\frac{\partial}{\partial X_{\alpha}} \left(N_{\alpha\beta} \frac{\partial u_3(X)}{\partial X_{\beta}} \right) \right] d\Omega(X) = \iint_{\Omega} U_{i3}(x', X) N_{\alpha\beta} \frac{\partial^2 u_3(X)}{\partial X_{\alpha} \partial X_{\beta}} d\Omega(X) \quad (4)$$

The alternative formulation in [32] employed the divergence theorem in the domain integral with the effect of GNL of eqn. (1) and did not use the additional condition for derivatives of in-plane forces ($N_{\alpha\beta,\alpha}=0$), as done in eqn. (4). The algebraic manipulation used in [32] is shown next:

$$\begin{aligned} & \iint_{\Omega} U_{i3}(x', X) \left[\frac{\partial}{\partial X_{\alpha}} \left(N_{\alpha\beta} \frac{\partial u_3(X)}{\partial X_{\beta}} \right) \right] d\Omega(X) = \dots \\ & = \int_{\Gamma} n_{\alpha}(x) N_{\alpha\beta}(x) u_{3,\beta}(x) U_{i3}(x', x) d\Gamma(x) - \iint_{\Omega} N_{\alpha\beta}(X) u_{3,\beta}(X) U_{i3,\alpha}(x', X) d\Omega(X) \quad (5) \end{aligned}$$

The final DBIE for buckling analyses using the alternative formulation in [32] is presented next:

$$\begin{aligned} & \frac{1}{2} C_{ij}(x') u_j(x') + \int_{\Gamma} [T_{ij}(x', x) u_j(x) - U_{ij}(x', x) t_j(x)] d\Gamma(x) = \dots \\ & = \int_{\Gamma} n_{\alpha}(x) N_{\alpha\beta}(x) u_{3,\beta}(x) U_{i3}(x', x) d\Gamma(x) - \iint_{\Omega} N_{\alpha\beta}(X) u_{3,\beta}(X) U_{i3,\alpha}(x', X) d\Omega(X) \end{aligned} \quad (6)$$

It is necessary to point out on the relation between the boundary integral with the GNL effect in eqn. (6) and the natural condition in the related part of the boundary when the deflection (u_3) is not prescribed. According to the result in eqn. (17) in [32], the boundary integral containing the effect of the GNL should only be computed along the boundary part with the prescribed deflection. The GNL effect requires the computation of the gradient of the deflection in the analysis. The BIE for the first derivative of the deflection in direction γ at an internal point is written next:

$$\begin{aligned} u_{3,\gamma}(X') &= \int_{\Gamma} \{n_{\alpha}(x) M_{3\alpha\beta,\gamma}(X', x) u_{\beta}(x) + n_{\beta}(x) Q_{3\beta,\gamma}(X', x) u_3(x) + \dots \\ & \dots - U_{3\beta,\gamma}(X', x) t_{\beta}(x) - U_{33,\gamma}(X', x) t_3(x)\} d\Gamma(x) - \int_{\Gamma} n_{\alpha}(x) N_{\alpha\beta}(x) u_{3,\beta}(x) U_{i3,\gamma}(X', x) d\Gamma(x) + \dots \\ & \dots + \iint_{\Omega} N_{\alpha\beta}(X) u_{3,\beta}(X) U_{33,\alpha\gamma}(X', X) d\Omega(X) \end{aligned} \quad (7)$$

Eqn. (7) was written with kernels differentiated with respect to the field point coordinates. The tangential differential operator can be introduced in kernels of integrals in eqn. (7) to reduce the singularities resulting from the differentiation as shown in [36].

The equation for the generalised plane stress problem is solved once to obtain the in-plane force distribution used in the buckling analysis. The BIEs for the plane stress problem are written next,

$$\frac{1}{2} C_{\alpha\beta}(x') v_{\beta}(x') + \int_{\Gamma} P_{\alpha\beta}(x', x) v_{\beta}(x) d\Gamma(x) = \int_{\Gamma} V_{\alpha\beta}(x', x) p_{\beta}(x) d\Gamma(x) \quad (8)$$

$$N_{\alpha\gamma}(X') = S_{\alpha\gamma\kappa\theta} \int_{\Gamma} \sigma_{\kappa\delta\beta}(X', x) D_{\theta\delta}[v_{\beta}(x)] d\Gamma(x) - \int_{\Gamma} \sigma_{\beta\alpha\gamma}(X', x) p_{\beta}(x) d\Gamma(x) \quad (9)$$

where v_{β} and p_{β} are the displacement and traction in direction β of the plane stress problem, respectively. $V_{\alpha\beta}$ and $P_{\alpha\beta}$ represent the displacement and traction in direction β due to a unit force in direction α , respectively. Eqn. (9) presents the BIE for stresses at internal points and was written with the tangential differential operator $D_{\alpha\beta}$ [44] and the Hooke tensor for isotropic media $S_{\alpha\beta\gamma\theta}$. The transversal modulus (G) is multiplied by the plate thickness in the generalised plane stress problem.

3 Application of the Dual Reciprocity Method

The kernels in the domain integral of the DBIEs (eqn. 6,7) contain the product between the gradient of deflection from the fundamental solution, the in-plane forces tensor and the gradient of the plate deflection. A vector function (b) resulting from the product between the in-plane forces tensor and the gradient of plate deflection can be defined, i.e.:

$$b_{\theta}(X) = N_{\theta\beta}(X)u_{3,\beta}(X) \quad (10)$$

The DRM is introduced in the approximation of the vector function (b) using the following relation [9]:

$$b_{\theta}(X) \simeq \sum_{m=1}^{N+L} \alpha_{\theta}^m f^m \quad (11)$$

The summation in eqn. (11) is extended along all points employed in the DRM, i.e. the total number of points placed on the boundary (N) and in the domain (L), f^m and α^m are sets of the approximating functions and weighting coefficients, respectively [9]. The relation between the particular solution \hat{u}_j^m and the approximating function f^m [9] is shown next:

$$\nabla^2(\nabla^2\phi) = \frac{1}{D}f(r) \quad (12)$$

$$\nabla^2(\hat{u}_3) = \frac{2}{D(1-\nu)\lambda^2}f(r) - \nabla^2\phi \quad (13)$$

$$\hat{u}_{\alpha} = \phi_{,\alpha} \quad (14)$$

Eqns. (12) to (14) are similar to those used to obtain the fundamental solution for the unit point load under the static condition in [36, 37] and the dynamic condition in [38]. Two types of radial basis functions f^m were considered here, and corresponding particular solutions for each adopted radial basis function are shown next:

$$f^m = 1 + r \Rightarrow \begin{cases} \hat{u}_{\alpha}^m = \frac{1}{D}\left(\frac{r^3}{16} + \frac{r^4}{45}\right)r_{,\alpha} \\ \hat{u}_3^m = \frac{2}{D(1-\nu)\lambda^2}\left(\frac{r^2}{4} + \frac{r^3}{9}\right) - \frac{1}{D}\left(\frac{r^4}{64} + \frac{r^5}{225}\right) \end{cases} \quad (15)$$

$$f^m = 1 + r + r^2 + r^3 \Rightarrow \begin{cases} \hat{u}_{\alpha}^m = \frac{1}{D}\left(\frac{r^3}{16} + \frac{r^4}{45} + \frac{r^5}{96} + \frac{r^6}{175}\right)r_{,\alpha} \\ \hat{u}_3^m = \frac{2}{D(1-\nu)\lambda^2}\left(\frac{r^2}{4} + \frac{r^3}{9} + \frac{r^4}{16} + \frac{r^5}{25}\right) - \frac{1}{D}\left(\frac{r^4}{64} + \frac{r^5}{225} + \frac{r^6}{576} + \frac{r^7}{1225}\right) \end{cases} \quad (16)$$

The result in eqn. (15) is similar to those presented in [17]. The distributed shear and bending moments related to the particular solutions are obtained with the constitutive equations (2) and (3). The generalised tractions are obtained from the distributed shear and bending moments according to relations presented next:

$$\begin{aligned}\hat{t}_\alpha^m &= \hat{M}_{\alpha\beta}^m n_\beta \\ \hat{t}_3^m &= \hat{Q}_\beta^m n_\beta\end{aligned}\quad (17)$$

The first derivative of the deflection ($U_{i3,\alpha}$) from the fundamental solution multiplies the term related to the effect of GNL in the DBIEs (eqn. 6). The introduction of the DRM to replace the domain integral requires the use of the BIE for the gradient of DBIEs. The BIE for the gradient of DBIEs with the kernel of the domain integral containing the function f^m and using the particular solution \hat{u}_j^m required to introduce the DRM [9] is shown next:

$$\begin{aligned}c\hat{u}_{i,\theta}^m(x') &= \int_\Gamma [n_\alpha(x)M_{i\alpha\beta,\theta}(x',x)\hat{u}_\beta^m(x) + n_\beta(x)Q_{i\beta,\theta}(x',x)\hat{u}_3^m(x) + \dots \\ &\dots - U_{i\beta,\theta}(x',x)\hat{t}_\beta^m(x) - U_{i3,\theta}(x',x)\hat{t}_3^m(x)]d\Gamma(x) - \iint_\Omega f^m(X)U_{i3,\theta}(x',X)d\Omega(X)\end{aligned}\quad (18)$$

Eqn. (18) was written with kernels differentiated with respect to the field coordinates, the scalar c is equal to 1 in case of collocation points located inside the domain and 0.5 in case of points placed on smooth parts of the boundary. The continuity of the first derivative of displacements at x' is required to apply eqn. (18) at points on the boundary. The DBIE for the buckling problem using eqn. (18) to introduce the DRM is given by:

$$\begin{aligned}&\frac{1}{2}C_{ij}(x')u_j(x') + \int_\Gamma [T_{ij}(x',x)u_j(x) - U_{ij}(x',x)t_j(x)]d\Gamma(x) = \dots \\ &= \int_\Gamma n_\alpha(x)N_{\alpha\beta}(x)u_{3,\beta}(x)U_{i3}(x',x)d\Gamma(x) + \sum_{m=1}^{N+L} \alpha_\theta^m \{c\hat{u}_{i,\theta}^m(x') + \dots \\ &\dots \dots - \int_\Gamma [n_\alpha(x)M_{i\alpha\beta,\theta}(x',x)\hat{u}_\beta^m(x) + n_\beta(x)Q_{i\beta,\theta}(x',x)\hat{u}_3^m(x) + \dots \\ &\dots - U_{i\beta,\theta}(x',x)\hat{t}_\beta^m(x) - U_{i3,\theta}(x',x)\hat{t}_3^m(x)]d\Gamma(x)\}\end{aligned}\quad (19)$$

The second derivatives of the deflection ($U_{33,\alpha\gamma}$) of the fundamental solution multiply the term related to the effect of GNL in the BIE for the gradient of the deflection (eqn. 7) used in the buckling analysis. The introduction of the DRM also requires the BIE for the second derivative of the deflection, as explained to obtain eqn. (19). The BIE for the second derivative of the deflection with the kernel of the domain integral containing f^m shown next:

$$\begin{aligned}c\hat{u}_{3,\gamma\theta}^m(x') &+ \int_\Gamma [n_\alpha(x)M_{3\alpha\beta,\gamma\theta}(x',x)\hat{u}_\beta^m(x) + n_\beta(x)Q_{3\beta,\gamma\theta}(x',x)\hat{u}_3^m(x) + \dots \\ &\dots - U_{3\beta,\gamma\theta}(x',x)\hat{t}_\beta^m(x) - U_{33,\gamma\theta}(x',x)\hat{t}_3^m(x)]d\Gamma(x) = \iint_\Omega f^m(X)U_{33,\gamma\theta}(x',X)d\Omega(X)\end{aligned}\quad (20)$$

Eqn. (20) was written with kernels differentiated with respect to the field coordinates, the scalar c is equal to 1 in case of collocation points located inside the domain and 0.5 in case of points placed on smooth parts of the boundary. The continuity of the second derivative of the deflection at x' is required to apply eqn. (20) at points on the boundary. The BIE for the gradient of the deflection using eqn. (20) to introduce the DRM is given next:

$$\begin{aligned}
gu_{3,\gamma}(x') = & \int_{\Gamma} \{n_{\alpha}(x)M_{3\alpha\beta,\gamma}(x',x)u_{\beta}(x) + n_{\beta}(x)Q_{3\beta,\gamma}(x',x)u_3(x) + \dots \\
& \dots - U_{3\beta,\gamma}(x',x)t_{\beta}(x) - U_{33,\gamma}(x',x)t_3(x)\}d\Gamma(x) - \int_{\Gamma} n_{\alpha}(x)N_{\alpha\beta}(x)u_{3,\beta}(x)U_{i3,\gamma}(x',x)d\Gamma(x) + \dots \\
& \dots + \sum_{m=1}^{N+L} \alpha_{\theta}^m \left\{ c\hat{u}_{i,\gamma\theta}^m(x') + \int_{\Gamma} [n_{\alpha}(x)M_{i\alpha\beta,\gamma\theta}(x',x)\hat{u}_{\beta}^m(x) + n_{\beta}(x)Q_{i\beta,\gamma\theta}(x',x)\hat{u}_3^m(x) + .. \right. \\
& \left. \dots - U_{i\beta,\gamma\theta}(x',x)\hat{t}_{\beta}^m(x) - U_{i3,\gamma\theta}(x',x)\hat{t}_3^m(x)]d\Gamma(x) \right\} \quad (21)
\end{aligned}$$

The scalar g in eqn. (21) has the same values explained to the scalar c in eqns. (18) and (20):

4 Numerical Implementation

The discretisation of the BIEs employed quadratic isoparametric boundary elements and the collocation points were always placed on the boundary. The same mapping function was used for conformal and non-conformal interpolations. The singularity subtraction [39] and the transformation of variable technique [40] were employed for the Cauchy and weak-type singularities, respectively, when integrations were performed on elements containing the collocation points. Hyper- and super-singular integrals in elements containing the collocation points were numerically evaluated using the computer code presented in [41]. The standard Gauss-Legendre scheme was employed for integrations on elements not containing the collocation points.

The DBIE for the buckling problem with the DRM used eqn. (19), which included a BIE for the gradient of deflections to introduce the DRM. The collocation points should be placed inside the boundary elements when using the BIE for the gradient. According to this requirement, the collocation points were placed at positions (-0.67 and 0.0), in the range (-1, 1), in the case of quadratic elements with continuity of displacements/tractions at the last node, which means that it was used to continuous elements or mixed type elements with continuity at the last node. On the other hand, the collocation points were placed at positions (-0.67, 0.0, +0.67) when the discontinuity of displacements/tractions appears at the last node, which means that it was employed to discontinuous elements or mixed elements with discontinuity at the last node. The position of the collocation point of the first node was always shifted inside the boundary elements (-0.67), which means continuous or discontinuous elements had collocations points inside irrespective of the continuity condition at the first node.

The DRM considered a uniform distribution of points in the domain. The DRM points on the boundary were always placed at the positions of the collocation points.

It is noted that the algebraic manipulation shown in eqn. (5) introduced one integral performed on the boundary, which is related to the effect of GNL but not with the DRM. The first boundary integral on the left hand side (LHS) of eqn. (19) results from eqn. (5), as well as the second boundary integral on the LHS of eqn. (21). The discretisation of those boundary integrals assumed a constant value along each boundary element for the sum of products between the derivatives of the deflection and the in-plane forces, which values were obtained at the central node. The values of derivatives of the deflection computed at the central node used by the DRM were also used in the computation of those boundary integrals related to eqn. (5)

The eigenvalue analysis used the basic inverse iteration with the Rayleigh quotient [42] as employed in [32] and summarised next:

$$Ax^{(k+1)} = Bx^k \quad (22)$$

$$\lambda_k = \frac{(x^{(k+1)}, x^k)}{(x^{(k+1)}, x^{(k+1)})} \quad (23)$$

The vector x^k is related to values of the first derivatives of the deflection at the centre of the cells. Eqn. (22) is the representation of the generalised eigenvalue problem and was not used explicitly; rather, the discretised forms of eqns. (19) and (21) were used, i.e. equations written in matrix form. Starting with an eigenvector x^1 with elements equal to 1.0, the values of the displacements and tractions at the nodes of the boundary elements are found with eqn. (19); these values are introduced in eqn. (21) to obtain the deflection derivatives (elements of the eigenvector x^2). The main difference with reference to the formulation using cell integration [32] appears in the need to computing elements α_{θ}^m . The elements of α are recalculated at each iteration step according to values of the first derivative of the deflection introduced in eqns. (10) and (11). After the computation of elements b_{θ} , the solution of the system of equations given by eqn. (11) carries the values of α_{θ}^m as explained in detail in [9]. The index θ in elements of b and α is related to directions in the plane of the plate, which means that eqns. (10) and (11) are used twice and one set of α is obtained for each direction θ of the plate.

5 Numerical Examples

The present study considered non-perforated plates and the results obtained are compared to those presented in the literature but considering those obtained in [32], where the buckling analysis considered the domain integration using cells. The results are presented in terms of the buckling parameter k , which is a non-dimensional value related to the critical load of plates (N_{cr}), the length of the plate side (a) and the flexural rigidity (D). The buckling parameter k was obtained according to the following relation:

$$k = \frac{a^2 N_{cr}}{\pi^2 D} \quad (24)$$

Uniform in-plane loads on the domain were assumed. The Young's modulus (E) and Poisson's ratio (ν) were 206.9 GPa and 0.3, respectively. The default value for the shear parameter κ^2 was $\pi^2/12$ for the Mindlin theory; otherwise, the value 5/6 was assigned when the results were obtained with the Reissner theory.

The results for square plates under in-plane loading in one direction are presented in Table 1, while those for loading in both directions are presented in Table 2, and those for in-plane pure shear load are presented in Table 3. The boundary conditions were simply supported edge (S), clamped edge (C) and free edge (F). The results obtained with simply supported and with clamped edges used the hard condition (rotation restrained in the tangent direction) for comparison with results from the literature. Results obtained with the DRM were presented in two rows of Tables 1, 2 and 3. The row with the label (DRM-f1) corresponds to results obtained with the function $(1+r)$ whereas that labelled (DRM-f2) is related to the function $(1+r+r^2+r^3)$. Different meshes were tested and the results presented in Tables 1 to 3 have differences of up to 3% to values in the literature (most of them have differences of only 1.5%). The values obtained with 256 cells [32] were included in the Tables but they were not used as the reference values to obtain the differences. The following meshes were used according to the Tables:

Table 1- 256 quadratic boundary elements (516 nodes) and 64 internal points;

Table 2- 384 quadratic boundary elements (772 nodes) and 256 internal points;

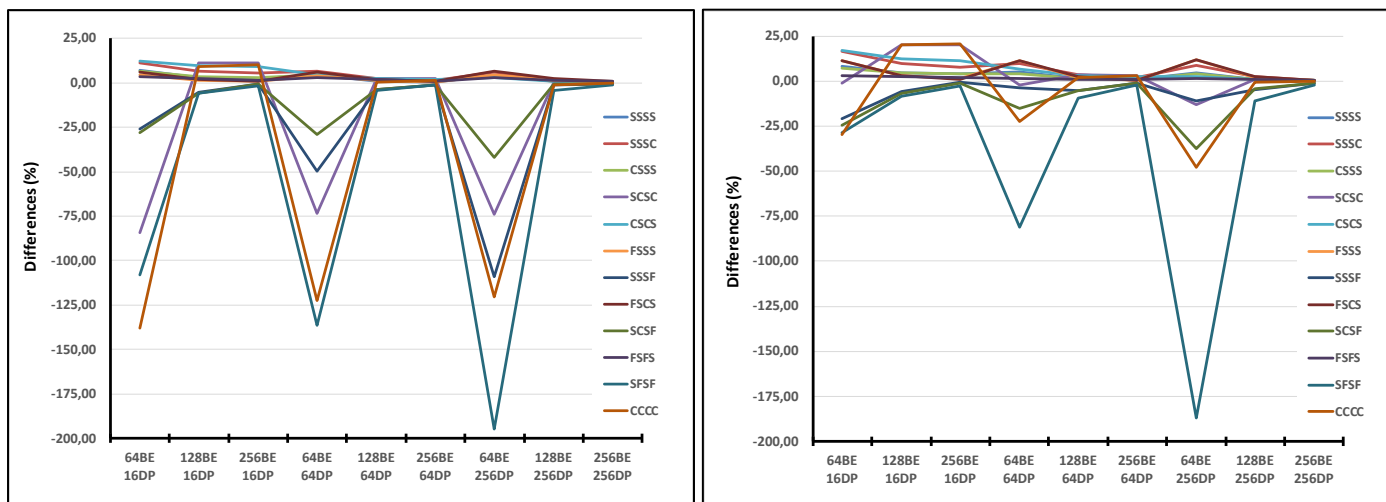
Table 3- 512 quadratic boundary elements (1028 nodes) and 256 internal points.

Table 1– Buckling parameter (k) of the first critical load of square plates under uniaxial in-plane loading

Type	h/a	[43]	Cells [32]	DRM-f1	DRM-f2
1) SSSS 	0.001	4.0000	4.0127	4.0191	4.0316
	0.010	3.9977*	4.0104	4.0169	4.0299
	0.050	3.9437	3.9561	3.9624	3.9726
	0.100	3.7838	3.7952	3.8009	3.8074
	0.200	3.2558	3.2643	3.2685	3.2740
2) SSSC 	0.001	4.8471	4.8707	4.9074	4.9314
	0.010	-	4.8665	4.8938	4.9122
	0.050	4.7454	4.7681	4.7941	4.8097
	0.100	4.4656	4.4858	4.5090	4.5206
	0.200	3.6115	3.6250	3.6419	3.6507
3) CSSS 	0.001	5.7401	5.7598	5.7767	5.7868
	0.010	-	5.7539	5.7619	5.7782
	0.050	5.5977	5.6164	5.6241	5.6423
	0.100	5.2171	5.2335	5.2399	5.2556
	0.200	4.1364	4.1572	4.1972	4.1596
4) SCSC 	0.001	6.7431	6.7967	6.8904	6.9542
	0.010	-	6.7875	6.8779	6.9424
	0.050	6.5238	6.5742	6.6609	6.7187
	0.100	5.9487	5.9914	6.0663	6.1129
	0.200	4.4004	4.4260	4.4762	4.5087
5) CSCS 	0.001	7.6911	7.7542	7.8471	7.8791
	0.010	-	7.7372	7.8327	7.8625
	0.050	7.2989	7.3561	7.4440	7.4675
	0.100	6.3698	6.4139	6.4853	6.5097
	0.200	4.3204	4.3413	4.3815	4.3942
6) FSSS 	0.001	1.4014**	1.4038	1.4072	1.4060
	0.010	1.4000**	1.4029	1.3992	1.3999
	0.050	1.3813**	1.3849	1.3811	1.3837
	0.100	1.3270**	1.3442	1.3404	1.3457
	0.200	1.2138**	1.2167	1.2133	1.2156
7) SSSF 	0.001	2.3639	2.3690	2.3399	2.3361
	0.010	-	2.3530	2.3464	2.3487
	0.050	2.2442	2.2520	2.2423	2.2446
	0.100	2.0829	2.0908	2.0791	2.0852
	0.200	1.7105	1.7178	1.7037	1.7060
8) FSCS 	0.001	1.6522	1.6555	1.6643	1.6592
	0.010	-	1.6536	1.6469	1.6471
	0.050	1.6197	1.6245	1.6176	1.6208
	0.100	1.5558	1.5604	1.5537	1.5613
	0.200	1.3701	1.3738	1.3683	1.3710
9) SCSF 	0.001	2.3901	2.3951	2.3650	2.3591
	0.010	-	2.3788	2.3717	2.3737
	0.050	2.2667	2.2747	2.2644	2.2662
	0.100	2.1010	2.1090	2.0968	2.1027
	0.200	1.7200	1.7274	1.7130	1.7151
10) FSFS 	0.001	0.9522	0.9537	0.9605	0.9588
	0.010	-	0.9532	0.9529	0.9549
	0.050	0.9431	0.9449	0.9446	0.9465
	0.100	0.9218	0.9236	0.9233	0.9252
	0.200	0.8501	0.8516	0.8512	0.8530
11) SFSF 	0.001	2.0413	2.0455	2.0152	1.9990
	0.010	-	2.0308	2.0239	2.0238
	0.050	1.9457	1.9508	1.9409	1.9397
	0.100	1.8216	1.8270	1.8156	1.8155
	0.200	1.5333	1.5389	1.5253	1.5255
12) CCCC 	0.001	10.0738***	10.1605	10.2300	10.3656
	0.010	-	10.1382	10.2764	10.3840
	0.050	9.5588***	9.6326	9.7637	9.8673
	0.100	8.2917***	8.3411	8.4547	8.5390
	0.200	5.3156***	5.3175	5.4807	5.4620

* [44], ** [3], *** [2]

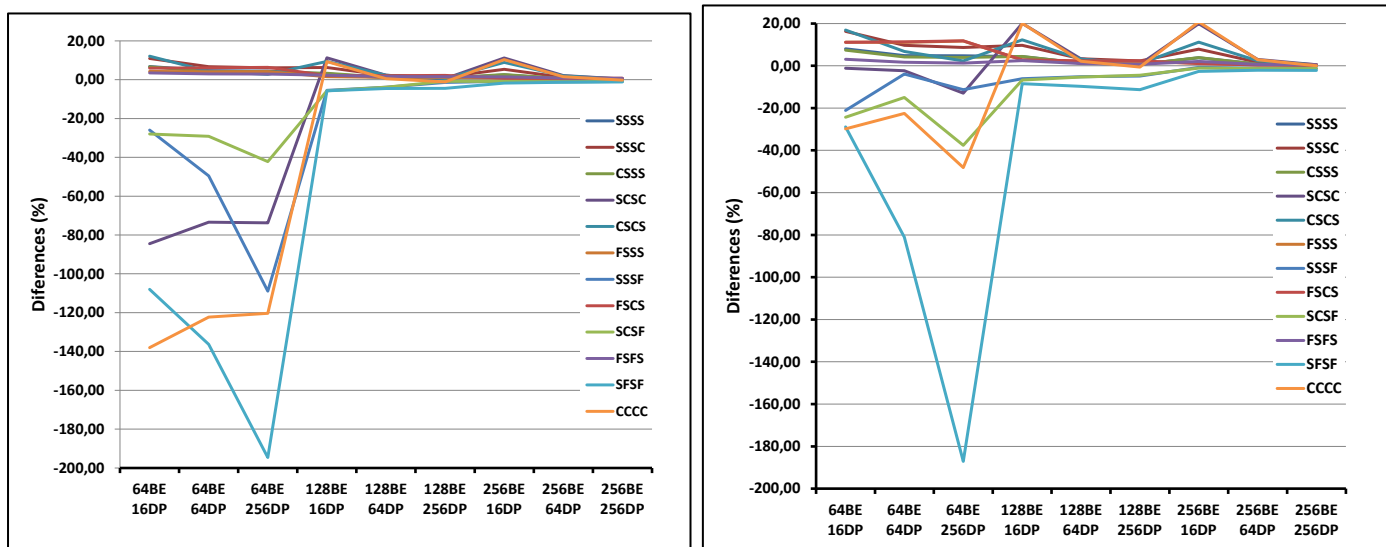
The behaviour of the DRM formulation with the in-plane loading in one direction (uniaxial loading) is shown in Figures 1 to 3. The analysis employed nine meshes obtained by combination of three sets of boundary elements (BE) (64, 128, 256) meshes with three sets of points in the domain (DP) (16, 64, 256).



a) $f=1+r$

b) $f=1+r+r^2+r^3$

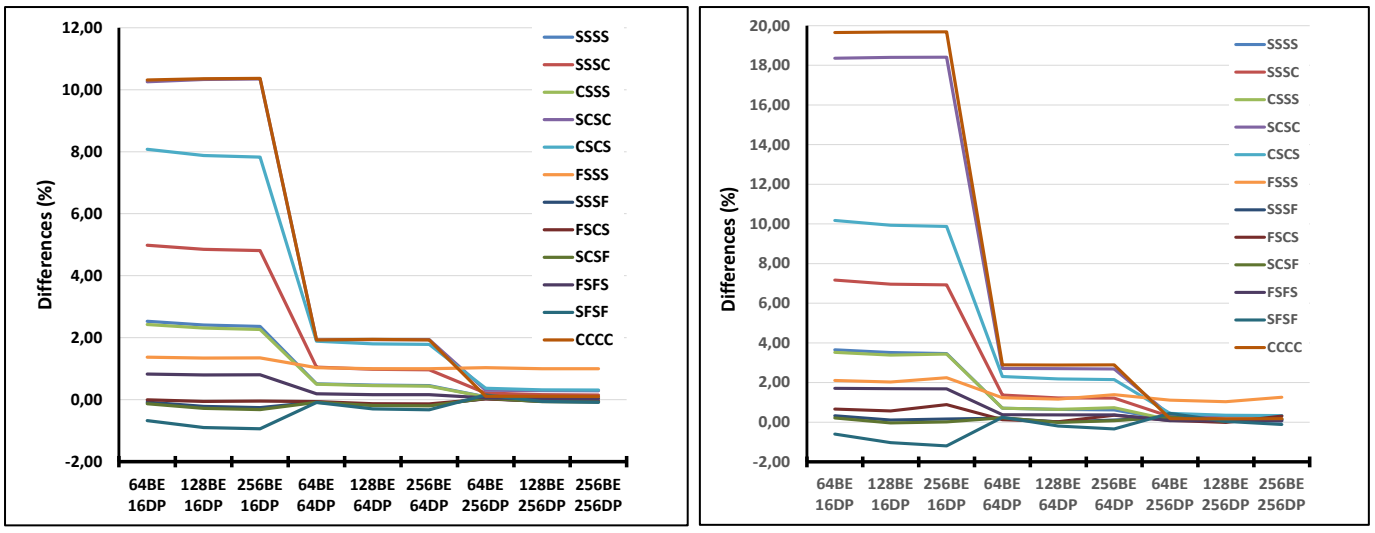
Figure 1- Uniaxial loading and $h/a=0.001$



a) $f=1+r$

b) $f=1+r+r^2+r^3$

Figure 2- Uniaxial loading and $h/a=0.05$



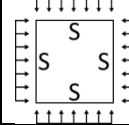
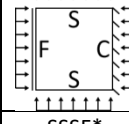
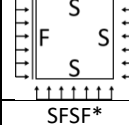
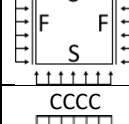
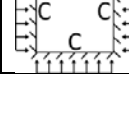
a) $f=1+r$

b) $f=1+r+r^2+r^3$

Figure 3- Uniaxial loading and $h/a=0.10$

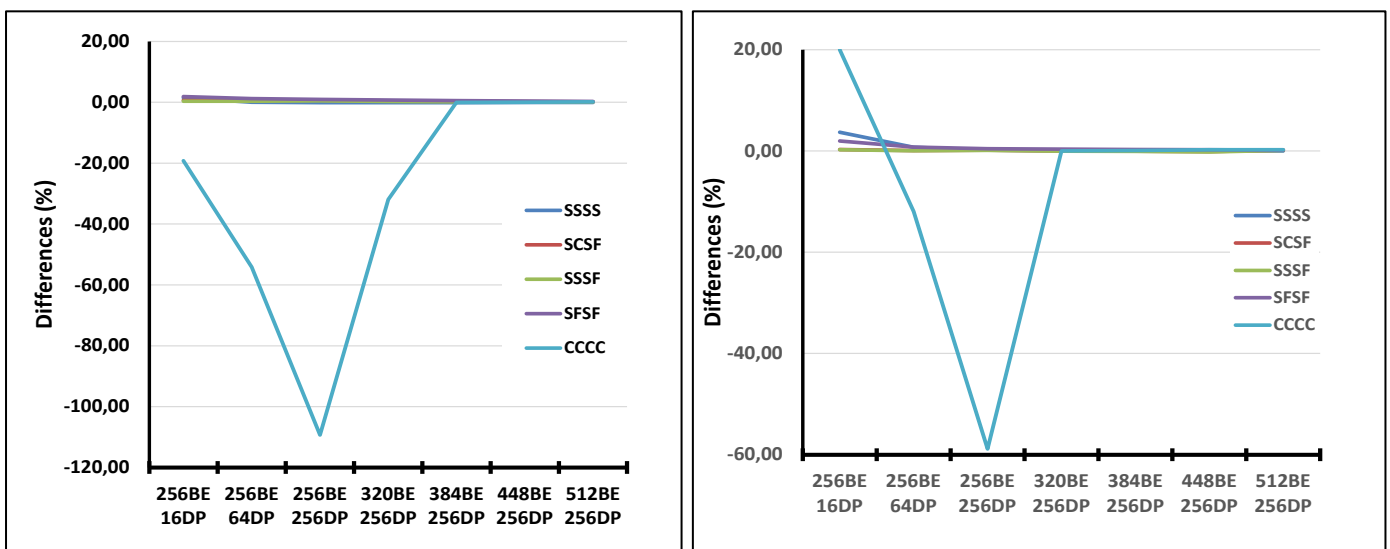
The results in Figures 1 to 3 were presented for ratios 0.001, 0.05 and 0.1. The ratio 0.05 was used instead of 0.01 because most of the reference results in Table 1 were not presented for 0.01. The authors checked the behaviour of ratio 0.01 using values from [32] and the behaviour was not very different to that with ratio 0.05. According to Figures 1 to 3, the increase in the number of boundary elements was necessary to reduce the difference for the ratio 0.001, whereas the increase in the number of domain points was necessary for other ratios. It is noted that the results in Figures 1 to 3 were organized to show this point. The behaviour for the ratio 0.2 was not presented because it was similar to those shown for ratios 0.05 and 0.1. On the other hand, the differences in the results obtained with the function $(1+r)$ were lower than those with the function $(1+r+r^2+r^3)$.

Table 2– Buckling parameter (k) of the first critical load of square plates under in-plane loading in both directions

Type	h/a	[43]	Cells [32]	DRM –f1	DRM – f2
 SSSS	0.001	2.0000	2.0064	1.9983	2.0014
	0.005	1.9997	2.0061	1.9983	2.0006
	0.050	1.9718	1.9782	1.9705	1.9727
	0.100	1.8919	1.8980	1.8907	1.8927
	0.150	1.7722	1.7780	1.7712	1.7729
 SCSF*	0.001	1.1431	1.1467	1.1470	1.1428
	0.005	1.1412	1.1449	1.1419	1.1408
	0.050	1.1119	1.1159	1.1119	1.1108
	0.100	1.0641	1.0680	1.0635	1.0624
	0.150	1.0049	1.0087	1.0037	1.0026
 SSSF*	0.001	1.0548	1.0576	1.0567	1.0540
	0.005	1.0535	1.0564	1.0534	1.0530
	0.050	1.0322	1.0354	1.0318	1.0311
	0.100	0.9954	0.9986	0.9945	0.9938
	0.150	0.9476	0.9507	0.9462	0.9456
 SFSF*	0.001	0.9321	0.9339	0.9373	0.9349
	0.005	0.9316	0.9335	0.9323	0.9325
	0.050	0.9207	0.9228	0.9214	0.9214
	0.100	0.8977	0.8998	0.8981	0.8982
	0.150	0.8650	0.8671	0.8651	0.8650
 CCCC	0.001	5.3036**	5.3482	5.3009	5.3087
	0.001	5.2970***	5.3460	5.3246	5.3234
	0.050	5.0840**	5.1254	5.1075	5.1055
	0.100	4.5400**	4.5741	4.5594	4.5577
	0.150	3.8727**	3.8992	3.8873	3.8861

* $\kappa^2=5/6$, ** [45], *** [46]

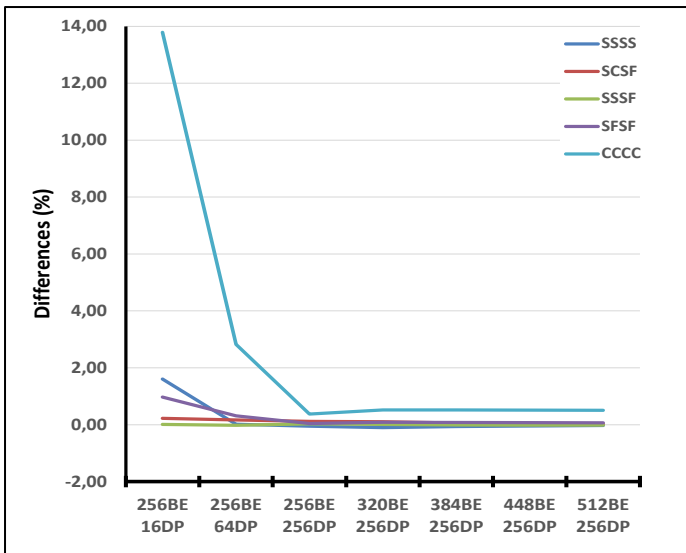
The behaviour of the formulation with the in-plane loading in both directions (biaxial loading) is shown in Figures 4 to 7. The analysis employed three meshes with 256 boundary elements (BE) and 16, 64, 256 points in the domain, four meshes with 256 domain points (DP) and having 320, 384, 440 and 512 boundary elements. According to Figures 4 to 7, the ratio 0.001 required more elements for the plate with all sides clamped. The function $(1+r+r^2+r^3)$ presented lower differences for a lower number of domain points for the ratio 0.001, whereas the function $(1+r)$ was better for other ratios.



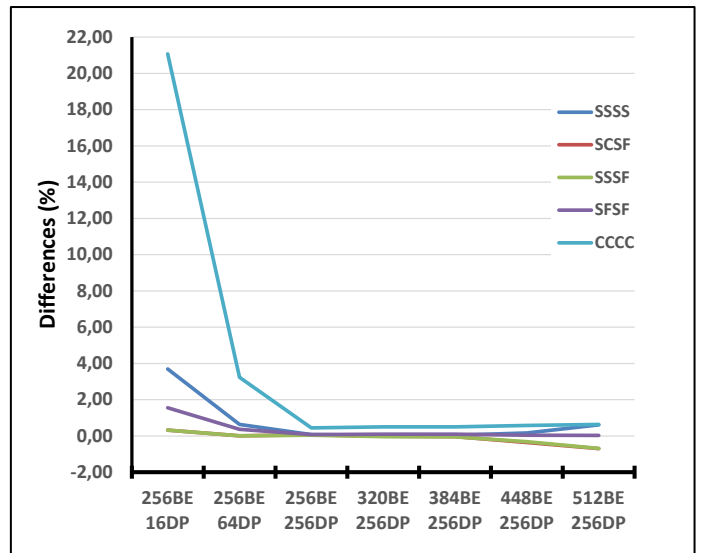
a) $f = 1+r$

b) $f = 1+r+r^2+r^3$

Figure 4- Biaxial loading and $h/a=0.001$

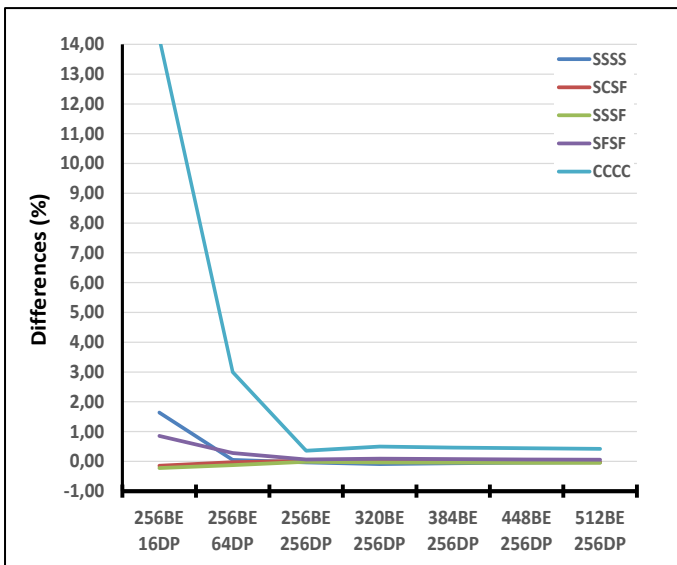


a) $f=1+r$

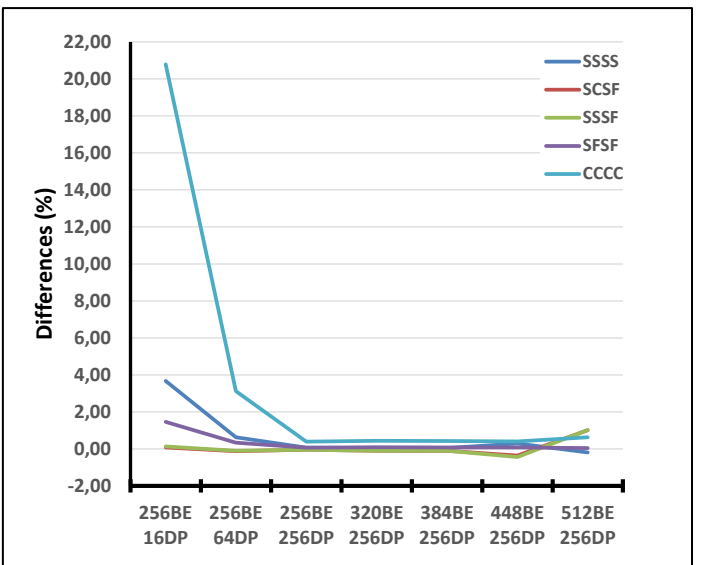


b) $f=1+r+r^2+r^3$

Figure 5- Biaxial loading and $h/a=0.005$

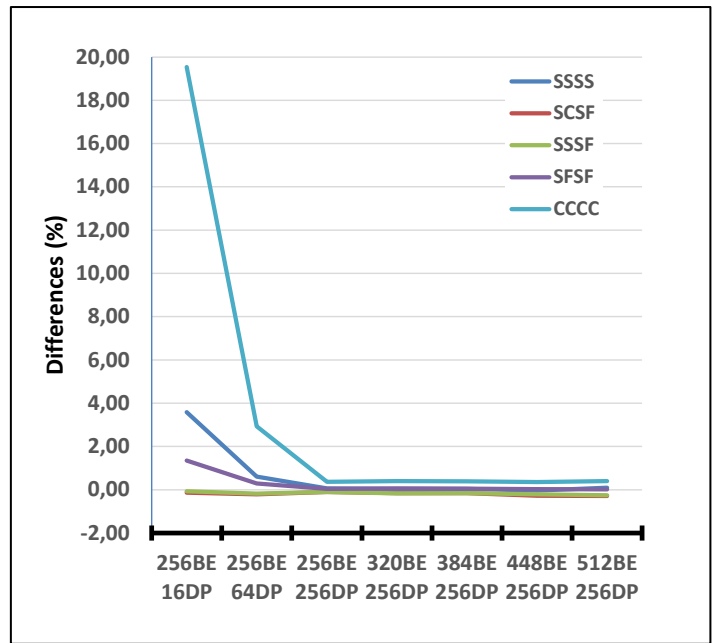
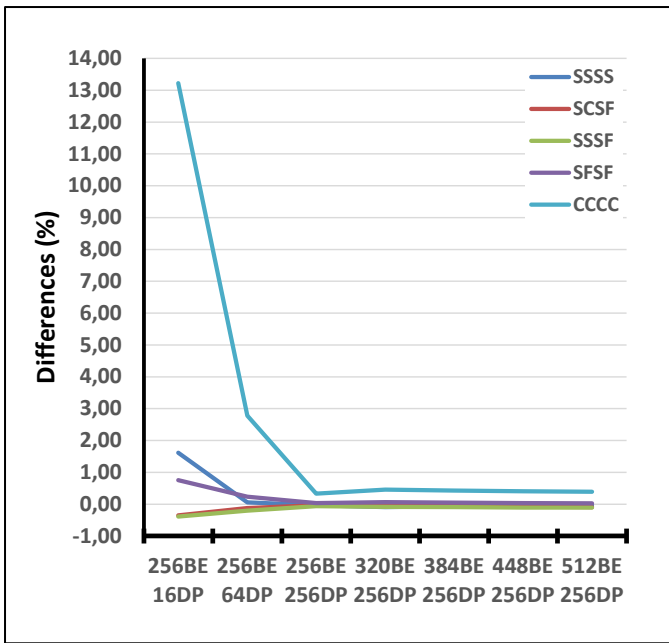


a) $f=1+r$



b) $f=1+r+r^2+r^3$

Figure 6- Biaxial loading and $h/a=0.05$



a) $f = 1+r$

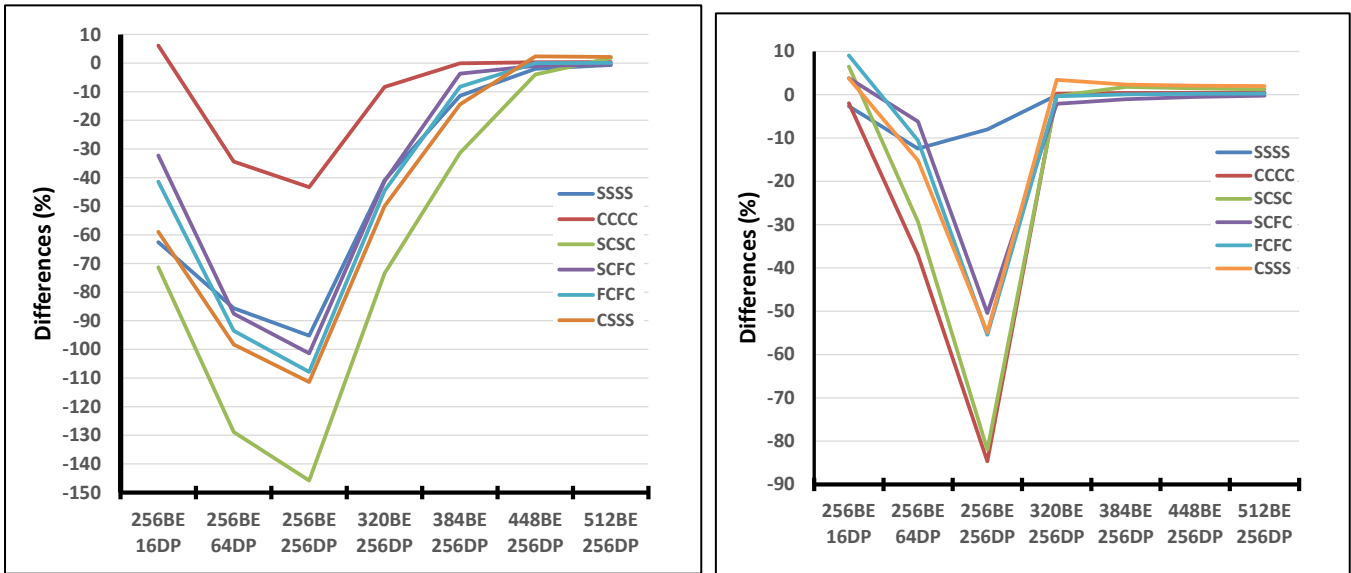
b) $f = 1+r+r^2+r^3$

Figure 7- Biaxial loading and $h/a=0.10$

Table 3– Buckling parameter (k) of the first critical load of plates under in-plane pure shear loading ($\kappa^2=5/6$, Reissner)

Type	h/a	Value in reference	Cells [32]	DRM -f1	DRM - f2
 SSSS	0.001	9.3400 (a)	9.4260	9.2794	9.3777
	0.01	9.3780 (b)	9.4083	9.3295	9.3557
	0.05		8.9979	8.9250	8.9457
	0.1		7.9201	7.8570	7.8686
	0.20		5.3269	5.2745	5.2766
 CCCC	0.001	14.7100 (a)	14.8702	14.7703	14.7760
	0.01	14.6155 (b)	14.8109	14.7154	14.7103
	0.05		13.5493	13.4506	13.4469
	0.1		10.8454	10.7417	10.7410
	0.20		6.1662	6.3455	6.3304
 SCSC	0.001	12.5997 (c)	12.7360	12.8363	12.7571
	0.01	12.5800 (d)	12.6947	12.6850	12.6551
	0.05		11.7923	11.7643	11.7408
	0.1		9.7344	9.6784	9.6679
	0.20		5.8436	5.8987	5.8582
 SCFC	0.001	8.4289 (e)	8.5001	8.3867	8.4103
	0.01		8.4398	8.3653	8.3710
	0.05		7.7706	7.6947	7.6996
	0.1		6.4888	6.4213	6.4244
	0.20		4.1638	4.1184	4.1192
 FCFC	0.001	7.4869 (e)	7.5437	7.4953	7.5067
	0.01		7.4938	7.4492	7.4516
	0.05		6.9230	6.8758	6.8778
	0.1		5.8095	5.7628	5.7646
	0.20		3.7634	3.7290	3.7299
 CSSS	0.001	10.6000 (f)	10.8349	10.8321	10.8142
	0.01		10.8083	10.7609	10.7604
	0.05		10.2089	10.1560	10.1553
	0.1		8.7375	8.6809	8.6794
	0.20		5.5783	5.5194	5.5193

(a) [47], (b) [48], (c) [49], (d) [50], (e) [51], (f) [13]



$$f=1+r$$

$$b) f=1+r+r^2+r^3$$

Figure 8- In-plane pure shear loading and $h/a=0.001$

The behaviour of the formulation for in-plane pure shear load is shown in Figure 8. The analysis employed three meshes with 256 boundary elements and 16, 64, 256 domain points, four meshes with 256 domain points and having 320, 384, 440 and 512 boundary elements, which were the same meshes used for the in-plane loading in both directions. The ratio 0.001 was used because it was the ratio with more reference values in Table 3. The function $(1+r+r^2+r^3)$ presented lower differences for this ratio and the convergence started with a lower number (320) of boundary elements than with the function $(1+r)$.

The results for rectangular plates under in-plane loading in one direction are presented in Table 4, those for loading in both directions are presented in Table 5, and those for in-plane pure shear load are presented in Table 6. The meshes had 64 boundary elements along the smaller side for uniaxial and biaxial loading, whereas those for shear loading had 128 boundary elements. The number of domain points was 256 irrespective of the ratio between the sides of the plate. The difference in results obtained to the reference values was up to 4%, but most of them were no higher than 1%.

Table 4a– Buckling parameter (k) of the first critical load of rectangular plates under uniaxial in-plane loading

a/b	h/a	[45]	Cells [32]	DRM	DIFF (%)	[45]	Cells [32]	DRM	DIFF (%)
0.5	0.001	6.2499	6.2995	6.2567	0.11	19.3380	19.8473	19.4529	0.59
0.5	0.050	6.0346	6.0807	6.0456	0.18	17.4347	17.6045	17.3410	-0.54
0.5	0.100	5.4693	5.5067	5.4784	0.17	13.2568	13.2916	13.0718	-1.40
0.5	0.150	4.7305	4.7581	4.7375	0.15	9.2233	9.3580	9.2946	0.77
1.0	0.001	4.0000	4.0127	4.0034	0.08	10.0737	10.1605	10.0458	-0.28
1.0	0.050	3.9437	3.9561	3.9463	0.07	9.5526	9.6326	9.5840	0.33
1.0	0.100	3.7839	3.7952	3.7862	0.06	8.2733	8.3375	8.3002	0.33
1.0	0.150	3.5446	3.5543	3.5465	0.05	6.7309	6.7769	6.8646	1.99
1.5	0.001	4.3406	4.3595	4.3595	0.44	8.3504	8.4152	8.4026	0.63
1.5	0.050	4.2559	4.2743	4.2670	0.26	7.9383	7.9973	7.9817	0.55
1.5	0.100	4.0214	4.0377	4.0312	0.24	6.9467	6.9930	6.9803	0.48
1.5	0.150	3.6831	3.6965	3.6911	0.22	5.7798	5.8130	5.8046	0.43
2.0	0.001	4.0000	4.0127	4.0185	0.46	7.8671	7.9538	8.1359	3.42
2.0	0.050	3.9437	3.9561	3.9543	0.27	7.4825	7.5353	7.7351	3.38
2.0	0.100	3.7839	3.7952	3.7933	0.25	6.5605	6.6056	6.6254	0.99
2.0	0.150	3.5446	3.5543	3.5524	0.22	5.4815	5.5117	5.5798	1.79

Table 4b– Buckling parameter (k) of the first critical load of rectangular plates under uniaxial in-plane loading

a/b	h/a	[52]	Cells [32]	DRM	DIFF (%)	[52]	Cells [32]	DRM	DIFF (%)
0.5	0.05	1.4696	1.4721	1.4678	-0.12	1.9464	1.9509	1.9444	-0.10
0.5	0.10	1.3416	1.3433	1.3388	-0.21	1.8233	1.8271	1.8202	-0.17
0.5	0.15	1.2080	1.2088	1.2042	-0.31	1.6839	1.6866	1.6796	-0.26
1.0	0.05	1.9464	1.9508	1.9444	-0.10	2.2452	2.2520	2.2433	-0.09
1.0	0.10	1.8233	1.8271	1.8201	-0.18	2.0852	2.0908	2.0815	-0.18
1.0	0.15	1.6839	1.6866	1.6791	-0.29	1.9035	1.9075	1.8981	-0.29
1.5	0.05	2.1466	2.1490	2.1427	-0.18	2.1920	2.1983	2.1883	-0.17
1.5	0.10	2.0007	2.0084	1.9950	-0.28	2.0421	2.0472	2.0363	-0.28
1.5	0.15	1.8753	1.8800	1.8264	-2.61	1.8705	1.8741	1.8628	-0.41
2.0	0.05	2.1522	2.1737	2.1458	-0.30	2.1960	2.2024	2.1902	-0.27
2.0	0.10	2.0085	2.0182	2.0119	0.17	2.0450	2.0502	2.0365	-0.41
2.0	0.15	1.8437	1.8442	1.8561	0.67	1.8725	1.8762	1.8618	-0.57
2.5	0.05	2.1903	2.2080	2.1958	0.25	2.1961	2.2024	2.1880	-0.37
2.5	0.10	2.0402	2.0549	2.0404	0.01	2.0451	2.0503	2.0336	-0.56
2.5	0.15	1.8689	1.8798	1.8639	-0.27	1.8725	1.8762	1.8583	-0.76
3.0	0.05	2.1920	2.1983	2.1845	-0.34	2.1960	2.2023	2.1850	-0.50
3.0	0.10	2.0421	2.0472	2.0300	-0.59	2.0450	2.0502	2.0297	-0.75
3.0	0.15	1.8705	1.8741	1.8552	-0.82	1.8725	1.8762	1.8538	-1.00

Table 4c– Buckling parameter (k) of the first critical load of rectangular plates under uniaxial in-plane loading

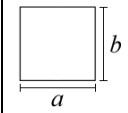
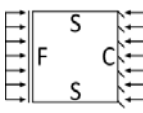
					
a/b	h/a	[52]	Cells [32]	DRM	DIFF (%)
0.5	0.05	2.4840	2.4932	2.4822	-0.07
0.5	0.10	2.2948	2.3022	2.2911	-0.16
0.5	0.15	2.0829	2.0883	2.0775	-0.26
1.0	0.05	2.2676	2.2747	2.2657	-0.09
1.0	0.10	2.1033	2.1090	2.0995	-0.18
1.0	0.15	1.9171	1.9212	1.9115	-0.29
1.5	0.05	2.2071	2.2136	2.2035	-0.16
1.5	0.10	2.0536	2.0589	2.0479	-0.28
1.5	0.15	1.8786	1.8823	1.8709	-0.41
2.0	0.05	2.1964	2.2027	2.1905	-0.27
2.0	0.10	2.0453	2.0504	2.0368	-0.41
2.0	0.15	1.8726	1.8764	1.8620	-0.57
2.5	0.05	2.1962	2.2025	2.1880	-0.37
2.5	0.10	2.0451	2.0503	2.0337	-0.56
2.5	0.15	1.8726	1.8763	1.8583	-0.77
3.0	0.05	2.1960	2.2024	2.1850	-0.50
3.0	0.10	2.0450	2.0502	2.0297	-0.75
3.0	0.15	1.8725	1.8762	1.8538	-1.00

Table 5a– Buckling parameter (k) of the first critical load of rectangular plates under in-plane loading in both directions

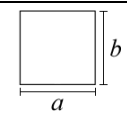
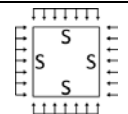
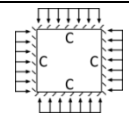
									
a/b	h/a	[45]	Cells [32]	DRM	DIFF (%)	[45]	Cells [32]	DRM	DIFF (%)
0.5	0.001	4.9999	5.0399	4.9902	-0.19	15.6930	16.0735	15.8062	0.72
0.5	0.050	4.8277	4.8659	4.8227	-0.10	13.9625	14.2662	14.1169	1.11
0.5	0.100	4.3754	4.4089	4.3716	-0.09	10.5408	10.7230	10.6282	0.83
0.5	0.150	3.7844	3.8122	3.7818	-0.07	7.5254	7.6309	7.5723	0.62
1.0	0.001	2.0000	2.0064	1.9966	-0.17	5.3036	5.3482	5.3007	-0.05
1.0	0.050	1.9719	1.9782	1.9689	-0.15	5.0840	5.1254	5.1130	0.57
1.0	0.100	1.8920	1.8980	1.8892	-0.15	4.5400	4.5741	4.5638	0.52
1.0	0.150	1.7723	1.7779	1.7699	-0.14	3.8727	3.8992	3.8907	0.47
1.5	0.001	1.4444	1.4478	1.4439	-0.04	4.1212	4.1482	4.1324	0.27
1.5	0.050	1.4297	1.4330	1.4292	-0.04	3.9879	4.0132	4.0116	0.59
1.5	0.100	1.3872	1.3904	1.3867	-0.03	3.6415	3.6628	3.6619	0.56
1.5	0.150	1.3218	1.3248	1.3213	-0.03	3.1898	3.2067	3.2059	0.51
2.0	0.001	1.2500	1.2525	1.2507	0.05	3.9234	3.9479	3.9456	0.57
2.0	0.050	1.2389	1.2414	1.2396	0.05	3.8046	3.8276	3.8405	0.95
2.0	0.100	1.2069	1.2093	1.2075	0.05	3.4906	3.5100	3.5216	0.89
2.0	0.150	1.1571	1.1593	1.1577	0.05	3.0725	3.0876	3.0975	0.81

Table 5b– Buckling parameter (k) of the first critical load of rectangular plates under in-plane loading in both directions

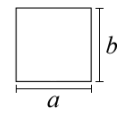
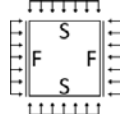
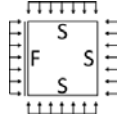
									
a/b	h/a	[52]	Cells [32]	DRM	DIFF (%)	[52]	Cells [32]	DRM	DIFF (%)
0.5	0.05	0.9080	0.9101	0.9101	0.22	1.1449	1.1492	1.1449	0.01
0.5	0.10	0.8875	0.8889	0.8892	0.19	1.0851	1.0893	1.0845	-0.06
0.5	0.15	0.8577	0.8592	0.8589	0.14	1.0155	1.0186	1.0143	-0.12
1.0	0.05	0.9207	0.9227	0.9217	0.11	1.0323	1.0352	1.0319	-0.036
1.0	0.10	0.8977	0.8995	0.8985	0.08	0.9954	0.9983	0.9947	-0.08
1.0	0.15	0.8651	0.8663	0.8654	0.04	0.9476	0.9497	0.9463	-0.14
1.5	0.05	0.9324	0.9344	0.9341	0.18	0.9930	0.9954	0.9927	-0.02
1.5	0.10	0.9086	0.9105	0.9100	0.15	0.9623	0.9648	0.9617	-0.07
1.5	0.15	0.8747	0.8760	0.8756	0.10	0.9208	0.9225	0.9196	-0.13
2.0	0.05	0.9408	0.9428	0.9431	0.25	0.9777	0.9799	0.9774	-0.03
2.0	0.10	0.9168	0.9192	0.9188	0.21	0.9496	0.9518	0.9488	-0.08
2.0	0.15	0.8824	0.8873	0.8838	0.16	0.9105	0.9121	0.9091	-0.15
2.5	0.05	0.9467	0.9500	0.9495	0.30	0.9709	0.9731	0.9707	-0.02
2.5	0.10	0.9226	0.9301	0.9590	3.94	0.9440	0.9461	0.9431	-0.10
2.5	0.15	0.8878	0.8992	0.8925	0.53	0.9061	0.9076	0.9044	-0.19
3.0	0.05	0.9509	0.9611	0.9548	0.42	0.9676	0.9697	0.9674	-0.03
3.0	0.10	0.9267	0.9645	0.9513	2.65	0.9414	0.9435	0.9403	-0.11
3.0	0.15	0.8917	0.9053	0.9121	2.29	0.9041	0.9055	0.9020	-0.23

Table 5c– Buckling parameter (k) of the first critical load of rectangular plates under in-plane loading in both directions

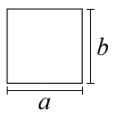
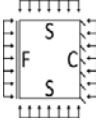
					
a/b	h/a	[52]	Cells [32]	DRM	DIFF (%)
0.5	0.05	1.7455	1.7549	1.7475	0.11
0.5	0.10	1.6222	1.6305	1.6226	0.02
0.5	0.15	1.4827	1.4887	1.4817	-0.07
1.0	0.05	1.1190	1.1299	1.1125	-0.58
1.0	0.10	1.0641	1.0677	1.0640	-0.01
1.0	0.15	1.0049	1.0075	1.0041	-0.08
1.5	0.05	1.0148	1.0175	1.0150	0.02
1.5	0.10	0.9807	0.9834	0.9804	-0.04
1.5	0.15	0.9356	0.9375	0.9346	-0.11
2.0	0.05	0.9860	0.9883	0.9860	0.00
2.0	0.10	0.9564	0.9588	0.9559	-0.06
2.0	0.15	0.9158	0.9175	0.9145	-0.14
2.5	0.05	0.9746	0.9757	0.9745	-0.01
2.5	0.10	0.9470	0.9622	0.9462	-0.08
2.5	0.15	0.9084	0.9254	0.9067	-0.18
3.0	0.05	0.9695	0.9705	0.9693	-0.01
3.0	0.10	0.9428	0.9573	0.9418	-0.10
3.0	0.15	0.9051	0.9215	0.9031	-0.23

Table 6a– Buckling parameter (k) of the first critical load of rectangular plates under in-plane pure shear loading

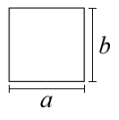
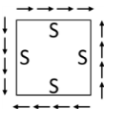
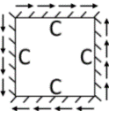
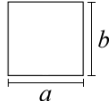
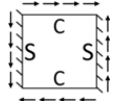
									
a/b	h/a	[47]	Cells [32]	DRM	DIFF (%)	[47]	Cells [32]	DRM	DIFF (%)
0.5	0.001		26.9274	26.0301			42.7394	41.6464	
0.5	0.050		23.9614	23.4259			33.6784	32.6510	
0.5	0.100		17.7443	17.2345			21.2577	20.4331	
0.5	0.150		12.2767	11.8205			13.3468	12.7129	
1.0	0.001	9.3400	9.4260	9.2794	-1.56	14.7100	14.8702	14.7703	-0.67
1.0	0.050		8.9979	8.9250			13.5493	13.4506	
1.0	0.100		7.9200	7.8570			10.8453	10.7417	
1.0	0.150		6.5963	6.5401			8.2270	8.1338	
1.5	0.001	7.1000	7.1254	7.1165	-0.13	11.5000	11.5923	11.5797	-0.11
1.5	0.050		6.8879	6.8811			10.9795	10.7549	
1.5	0.100		6.2612	6.2517			9.1297	8.9411	
1.5	0.150		5.4326	5.4195			7.1367	7.0475	
2.0	0.001	6.6000	6.6162	6.6538	0.57	10.3400	10.3581	10.4093	0.49
2.0	0.050		6.4089	6.4271			9.6753	9.7178	
2.0	0.100		5.8428	5.8568			8.1421	8.1628	
2.0	0.150		5.0902	5.0986			6.5061	6.5107	

Table 6b– Buckling parameter (k) of the first critical load of rectangular plates under in-plane pure shear loading

					
a/b	h/a	[47]	Cells [32]	DRM	DIFF (%)
0.5	0.001		27.6157	26.9096	
0.5	0.050		24.9439	23.9350	
0.5	0.100		18.4455	17.8668	
0.5	0.150		12.4725	11.9802	
1.0	0.001	12.2800	12.7360	12.8346	0.77
1.0	0.050		11.7916	11.7647	
1.0	0.100		9.7340	9.6786	
1.0	0.150		7.6082	7.5402	
1.5	0.001	11.1200	10.9085	10.8919	-0.15
1.5	0.050		10.1715	10.1476	
1.5	0.100		8.5249	8.4940	
1.5	0.150		6.7780	6.7462	
2.0	0.001	10.2100	10.1129	10.1544	0.41
2.0	0.050		9.4649	9.5008	
2.0	0.100		8.0000	8.0168	
2.0	0.150		6.4202	6.4234	

6 Conclusions

The application of the DRM in the formulation presented in [32] for buckling analysis was carried out in this study. Simple radial basis functions f^m were considered to approximate the effect of GNL on the domain and no shape parameter was adopted as well as no additional numerical strategy or tool was used to improve the convergence or the integrations over the boundary elements. The behaviour of the DRM considering both radial basis functions was comparable to the solution in [32], which employed constant cells in the domain to perform the domain integration. It was the reason to do not using other radial basis functions f^m in the present analysis. According to Figures 1 to 8, the number of boundary elements had to be increased with reference to boundary element meshes employed in [32]. The role of increasing the number of boundary elements in the DRM is to improve the boundary integration which replaces the domain integration. In spite of the identity in eqns. (18) and (20) of the domain integral containing the radial basis function to equivalent boundary integrals, the integration of domain cells in [32] has worked with functions U_{i3} or $U_{33,\gamma}$, which have logarithmic and $1/r$ singularity types, respectively, when the field point approaches the collocation point. The equivalent boundary integrals in the DRM have kernels contained hyper- and super-singularities beyond the logarithmic and $1/r$ singularities. The analyses considering the ratio h/a equal to 0.001 required more boundary elements in the present analysis using DRM as well as in the analyses presented in [32]. According to the literature on buckling analyses, this ratio should be considered in the evaluation of bending models containing the effect of shear deformation when the results are compared to values from the classical bending model;

The authors believe this DRM formulation for buckling analysis presented a consistent behaviour and accurate results. On the other hand, the cost of the present formulation, which works with three types of BIEs, i.e. the displacement, the gradient and that for the second derivative, are acceptable in the DRM formulation. The BIE for the second derivative was used to approximate the GNL effect in the domain to equivalent boundary integrals rather than to introduce the effect of GNL in the DBIE, which happens in the buckling formulation during the algebraic manipulation shown in eqn. (4).

The use of simple radial basis function ($1+r$) to introduce the DRM was the target of this study on plate buckling considering the effect of shear deformation. The results were compared with those in [32] where a similar BEM formulation used constant cells in the domain discretization to perform the integration. An alternate radial basis function ($1+r+r^2+r^3$) obtained with the addition of terms on the simple function presented results slightly better than ($1+r$) only in few cases. In general, the behaviour of the simple function ($1+r$) was stable and better results are obtained when the number of points for DRM and boundary elements were increased in all cases as happened in [32] with reference to the increase of the number of constant cells on the domain.

Acknowledgements

The authors are grateful to CNPq (305997/2016-5) and CAPES (01P03713/2017) for their support in the development of this research.

References

1. Timoshenko SP, Woinowsky-Krieger S. Theory of Plates and Shells, McGraw-Hill Book Company, New York, 2nd Ed., 1959.
2. Kitipornchai S, Xiang Y. Buckling of thick skew plates, International Journal of Numerical Methods in Engineering, v. 36, p. 1299-1310, 1993.
3. Mizusawa T. Buckling of rectangular Mindlin plates with tapered thickness by the spline strip method, International Journal of Solids & Structures, v. 30, n. 12, pp. 1663-1677, 1993.
4. Reissner E. The effect of transverse shear deformation on the bending of elastic plates, Journal of Applied Mechanics, v. 12, n. 2, p. A66-A77, 1945.
5. Mindlin RD. Influence of rotatory inertia and shear on flexural motions of isotropic elastic plates, Journal of Applied Mechanics, v. 18, p. 18-31, 1951.
6. Nardini D, Brebbia CA. A new approach to free vibration analysis using boundary elements. Applied Mathematical Modelling, v. 7, n. 3, p. 157-162, 1983.
7. Brebbia CA, Nardini D. Dynamic analysis in solid mechanics by an alternative boundary element procedure. International Journal of Soil Dynamics and Earthquake Engineering, v. 2, n. 4, p. 228-233, 1983.
8. Nardini D, Brebbia CA. Boundary integral formulation of mass matrices for dynamic analysis. In: Time-dependent and Vibration Problems. Springer, Berlin, Heidelberg, p. 191-208, 1985.
9. Partridge PW, Brebbia CA, Wrobel LC. The Dual Reciprocity Boundary Element Method, Computational Mechanics Publication and Elsevier Applied Science, London and New York, 1992.
10. Kamiya N, Sawaki Y. The plate bending analysis by the dual reciprocity boundary elements. Engineering Analysis with Boundary Elements, v. 5, n. 1, p. 36-40, 1988.
11. Silva NA, Venturini WS. Dual reciprocity process applied to solve bending plates on elastic foundations. Boundary Element X, v. 3, p. 95-106, 1988.
12. Sawaki Y, Takeuchi K, Kamiya N. Nonlinear bending analysis without domain-cell discretisation. Engineering Analysis with Boundary Elements, v. 7, n. 3, p. 130-135, 1990.
13. Elzein A, Syngellakis S. The dual reciprocity in boundary element formulations of the plate buckling problem. Engineering Analysis with Boundary Elements, v. 9, n. 2, p. 175-184, 1992.
14. Davies TW, Moslehy FA. Modal analysis of plates using the dual reciprocity boundary element method. Engineering Analysis with Boundary Elements, v. 14, n. 4, p. 357-362, 1994.

15. Lin J, Duffield, RC, Shih H. Buckling analysis of elastic plates by boundary element method. *Engineering Analysis with Boundary Elements*, v. 23, n. 2, p. 131-137, 1999.
16. Wen PH, Aliabadi MH, Young A. Transformation of domain integrals to boundary integrals in BEM analysis of shear deformable plate bending problems. *Computational Mechanics*, v. 24, n. 4, p. 304-309, 1999.
17. Wen PH; Aliabadi MH; Young A. Application of dual reciprocity method to plates and shells. *Engineering Analysis with Boundary Elements*, v. 24, n. 7-8, p. 583-590, 2000.
18. Wang W, Ji X, Tanaka M. A dual reciprocity boundary element approach for the problems of large deflection of thin elastic plates. *Computational Mechanics*, v. 26, n. 1, p. 58-65, 2000
19. Wen PH, Aliabadi MH, Young A. Large deflection analysis of Reissner plate by boundary element method. *Computers & Structures*, v. 83, n. 10-11, p. 870-879, 2005.
20. Purbolaksono J, Aliabadi MH. Large deformation of shear deformable plate by boundary element method. *Journal of Engineering Mathematics*, v. 51, p. 211–230, 2005.
21. Supriyono, Aliabadi MH. Analysis of shear deformable plates with combined geometric and material nonlinearities by boundary element method. *International Journal of Solids and Structures*, v. 44, n. 3-4, p. 1038-1059, 2007.
22. Purbolaksono J, Aliabadi MH. Stability of Euler's method for evaluating large deformation of shear deformable plates by dual reciprocity boundary element method. *Engineering Analysis with Boundary Elements*, v. 34, n. 9, p. 819-823, 2010.
23. Yan F, Feng X, Zhou H. dual reciprocity hybrid radial boundary node method for the analysis of Kirchhoff plates. *Applied Mathematical Modelling*, v. 35, n. 12, p. 5691-5706, 2011.
24. Purbolaksono J, Dirgantara T, Aliabadi MH. Fracture mechanics analysis of geometrically nonlinear shear deformable plates. *Engineering Analysis with Boundary Elements*, v. 36, n. 2, p. 87-92, 2012.
25. Useche J, Albuquerque EL. Dynamic analysis of shear deformable plates using the dual Reciprocity Method. *Engineering Analysis with Boundary Elements*, v. 36, n. 5, p. 627-632, 2012.
26. Di Pisa C., Aliabadi MH. Fatigue crack growth analysis of assembled plate structures with dual boundary element method. *Engineering Fracture Mechanics*, v. 98, p. 200-213, 2013.
27. Useche J. Vibration analysis of shear deformable shallow shells using the Boundary Element Method. *Engineering Structures*, v. 62, p. 65-74, 2014.
28. Pomeranz SB, Hamill WA. Dual reciprocity versus Bessel function fundamental solution boundary element methods for the plane strain deformation of a thin plate on an elastic foundation. *Engineering Analysis with Boundary Elements*, v. 41, p. 37-46, 2014.
29. Uğurlu B. A dual reciprocity boundary element solution method for the free vibration analysis of fluid-coupled Kirchhoff plates. *Journal of Sound and Vibration*, v. 340, p. 190-210, 2015.
30. Useche J, Albuquerque EL. Transient dynamic analysis of shear deformable shallow shells using the boundary element method. *Engineering Structures*, v. 87, p. 1-7, 2015.
31. Useche J, Harnish C. A boundary element method formulation for modal analysis of doubly curved thick shallow shells. *Applied Mathematical Modelling*, v. 40, n. 5-6, p. 3591-3600, 2016.
32. Soares Jr RA, Palermo Jr L. Effect of shear deformation on the buckling parameter of perforated and non-perforated plates studied using the boundary element method, *Engineering Analysis with Boundary Elements*, v85, 57–69, 2017.
33. Lei XY, Huang MK, Wang XX. Geometrically nonlinear analysis of a Reissner's type plate by boundary element method, *Comput Struct*; 37(6):911–16, 1990.

34. Palermo Jr L. The tangential differential operator applied to a stress boundary integral equation for plate bending including the shear deformation effect. *Engineering Analysis with Boundary Elements*, v. 36, p. 1213-1225, 2012.
35. Bonnet M. *Boundary Integral Equation Methods for Solids and Fluids*. John Wiley & Sons Ltd; 1999.
36. Palermo Jr L. A study about fundamental solutions in plates. 22nd Conference on the Boundary Element Method (BEM 22) p. 373–84, 2000.
37. Palermo Jr L. Plate bending analysis using the classical or the Reissner–Mindlin models. *Engineering Analysis with Boundary Elements*, V. 27, p. 603-609, 2003.
38. Palermo Jr L. On the harmonic response of plates with the shear deformation effect using the elastodynamic solution in the boundary element method. *Engineering Analysis with Boundary Elements*, v. 31, p. 176-183, 2007.
39. Aliabadi M.H. *The Boundary Element Method: Applications in Solids and Structures*, John Wiley & Sons Ltd., 2002.
40. Telles JCF. A self-adaptive coordinate transformation for efficient numerical evaluation of general boundary element integrals, *Int. J. Num. Meth. Eng.*, v. 24, p. 959-973, 1987.
41. Gao X. Numerical evaluation of two-dimensional singular boundary integrals—Theory and Fortran code, *Journal of Computational and Applied Mathematics*, v. 188, p. 44–64, 2006.
42. Wilkinson J.H. *The Algebraic Eigenvalue Problem*, Oxford University Press, William Clowes & Sons, London, 1972.
43. Hosseini-Hashemi S, Khorshidi K, Amabili M. Exact solution for linear buckling of rectangular Mindlin plates. *Journal of Sound and Vibration*, v. 315, n. 1, p. 318-342, 2008.
44. Hosseini-Hashemi S, Atashipour SR, Fadaee M. On the buckling analysis of isotropic, transversely isotropic, and laminated rectangular plates via Reddy plate theory: an exact closed-form procedure. *Proceedings of the Institution of Mechanical Engineers, Part C: Journal of Mechanical Engineering Science*, v. 226, n. 5, p. 1210-1224, 2012
45. Xiang Y, Wang CM, Liew KM, Kitipornchai S, Mindlin plate buckling with prebuckling in-plane deformation. *Journal of Engineering Mechanics*, v. 119, n. 1, p. 1-18, 1993.
46. Dawe DJ, Roufaeil OL. Buckling of rectangular Mindlin plates, *Computers & Structures*, v.15, n.4, p. 461-471, 1982.
47. Timoshenko SP, Gere JM. *Theory of Elastic Stability*, 2nd Ed. Dover Publication, New York, 1961.
48. Bui TQ, Nguyen, MN, Zhang C. Buckling analysis of Reissner-Mindlin plates subjected to in-plane edge loads using a shear-locking-free and meshfree method. *Engineering Analysis with Boundary Elements*, v. 35, n. 9, p. 1038-1053, 2011.
49. Vrcelj Z, Bradford MA. A simple method for the inclusion of external and internal supports in the spline finite strip method (SFSM) of buckling analysis. *Computers & Structures*, v. 86, n. 6, p. 529-544, 2008.
50. Tham L, Szeto H. Buckling analysis of arbitrarily shaped plates by spline finite strip method, *Computers & Structures*, v. 36, n. 4, p. 729-735, 1990.
51. Shufrin I, Eisenberger M. Shear buckling of thin plates with constant in-plane stresses. *International Journal of Structural Stability and Dynamics*, v. 7, n. 2, p. 179-192, 2007.
52. Liew KM, Xiang Y, Kitipornchai S. Analytical buckling solutions for Mindlin plates involving free edges, *International Journal of Mechanical Sciences*, v. 38, n. 10, p. 1127-1138, 1996.